Journal of Colloid and Interface Science 678 (2025) 1075–1086

Contents lists available at ScienceDirect

Journal of Colloid And Interface Science

journal homepage: www.elsevier.com/locate/jcis

Regular Article

Wetting characterisation on complex surfaces by an automatic open-source tool: DropenVideo

Raziyeh Akbari [a,*], Federico Ambrosio [a], Joseph D. Berry [b], Carlo Antonini [a,*]

[a] Department of Materials Science, University of Milano-Bicocca, via R. Cozzi 55, 20125 Milano, Italy
[b] School of Chemical and Biomedical Engineering, The University of Melbourne, Parkville, Victoria 3010, Australia

GRAPHICAL ABSTRACT

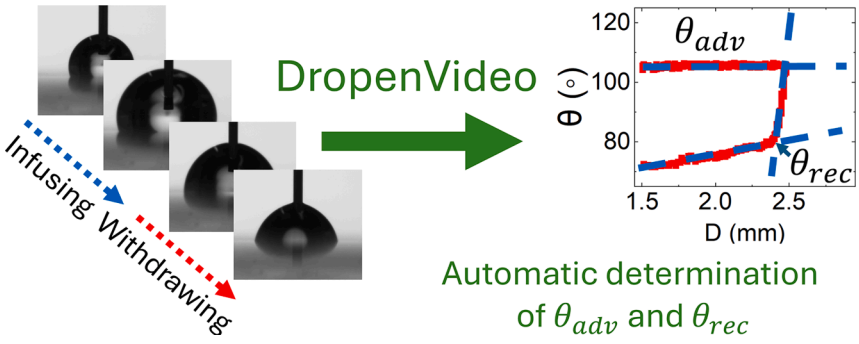

ARTICLE INFO

Keywords:
Wetting
Contact angle
Image analysis
MATLAB
Open-source
DropenVideo

ABSTRACT

Hypothesis: Investigating solid–liquid interactions to determine advancing and receding contact angles, and consequently contact angle hysteresis, is crucial for understanding material wetting properties. A reliable, automated, and possibly open-source tool is desirable, to standardize and automatize the measurement and make it user-independent.

Experiments: This study introduces an open-source software, DropenVideo, as an extension of Dropen. DropenVideo automates frame-by-frame video analysis for the advancing and receding contact angle determination, by considering needle presence, contrast tuning, and compensating for missing drop edge data. Contact angles are calculated using convolution mask, circle, and polynomial fittings. An innovative feature in DropenVideo is the automatic protocol for identifying advancing and receding contact angles: (i) the advancing contact angle is determined as the average value during drop inflation; and (ii) the receding contact angle is determined from the frame of incipient motion during drop deflation.

Findings: Exploring the application of DropenVideo across a range of complex surfaces as representative test cases, we highlight existing challenges in interpreting wetting measurements by addressing different wetting scenarios. Our study demonstrates that employing frame-by-frame automatic analysis of contact angle measurement videos using DropenVideo significantly mitigates the potential risks of subjective bias associated with manual interpretation and enhances the precision of identified wetting characteristics.

* Corresponding authors.
E-mail addresses: raziyeh.akbari@unimib.it (R. Akbari), carlo.antonini@unimib.it (C. Antonini).

https://doi.org/10.1016/j.jcis.2024.08.159
Received 24 April 2024; Received in revised form 26 July 2024; Accepted 19 August 2024
Available online 27 August 2024

1. Introduction

Interpretation of wetting properties of a solid in contact with a liquid is not always straightforward due to complex liquid–solid interactions. One of the first and most commonly used parameters to characterize solid–liquid interaction is the contact angle. Liquid repellence and mobility on a surface depend on contact angles and contact angle hysteresis ($\Delta\theta$), equal to the difference between the advancing (θ_{adv}) and receding (θ_{rec}) contact angles. Contact angle hysteresis was introduced in the early 20th century by Rayleigh and Pockels [1,2]. A comprehensive understanding and control of $\Delta\theta$ enable the design of materials and surfaces tailored to specific wetting requirements across a wide range of applications. For instance, in the context of self-cleaning surfaces, a low $\Delta\theta$ would promote the easy shedding of water drops and particulate contaminants. In microfluidics, $\Delta\theta$ is a valuable tool for controlling the movement of liquid within intricate microfluidic channels [3,4].

Despite extensive research conducted on wetting since the concept of the contact angle was introduced by Thomas Young in 1805, the understanding of various aspects of contact angle remains unclear [1]. When considering the propagation velocity of the liquid contact line on the surface during a wetting experiment in lab, the contact angle can be categorized into static, quasi-static and dynamic types [2,5]. A static contact angle is measured when the droplet is gently placed on the surface with negligible subsequent drop movement. In contrast, the quasi-static and dynamic contact angles may vary with liquid infusion and withdrawing rates, drop size, and surface characteristics. The presence of multiple local minima in the Gibbs free energy of the liquid–solid interaction [3,6], leads to variations in the measured contact angles in the laboratory, resulting in the absence of a single, definitive value. As such, none of the measured contact angles in the laboratory is the equilibrium contact angle. Therefore, thermodynamically derived wetting models like Young, Wenzel, and Cassie-Baxter are not always applicable to the laboratory findings [1,7–11].

Contact angles are vital for understanding drop adhesion on solid surfaces. Specifically, the total frictional force due to capillarity scales as $F \propto \gamma R(\cos\theta_R - \cos\theta_A)$ [12,13], or from a recent derivation by McHale et al. scales as $F \propto \gamma R \Delta\theta \sin\theta_e$ [14] where γ is the liquid surface tension, R is the drop dimension, and θ_e is the liquid equilibrium contact angle on the surface. These scalings imply that lowest adhesion is achieved when both contact angles are high and the hysteresis is low, not just for a low hysteresis [15]. Strictly speaking, θ_{adv} and θ_{rec} represent the contact angles in the moment of the incipient motion of the contact line during wetting and de-wetting of the substrate, respectively. Practically, the contact angle is normally constant as the contact line quasi-statically advances, e.g. during drop expansion, and equal to θ_{adv}. Conversely, θ_{rec} is more challenging to measure, as the contact angle is often not constant as the contact line recedes, e.g. during drop contraction [16,17]. Experimental investigations revealed that both static and dynamic components exist simultaneously in the experimentally measured $\Delta\theta$ due to the substantial influence of contact line velocity on both θ_{adv} and θ_{rec} [2,3]. The static component is partially applicable to thermodynamic models, whereas the dynamic or kinetic component is not [2]. Due to the presence of many local extrema in the Gibbs free energy, $\Delta\theta$ is present even on an homogeneous, flat, inert, and smooth solid surface [2]. Surface roughness, chemical heterogeneity, and the formation of interfacial bonds between the liquid and the solid can increase $\Delta\theta$ due to contact line pinning at surface irregularities and asperities [1,16].

Some of the commonly employed methods to measure $\Delta\theta$ are represented in Fig. 1, similar to those employed in the study of adaptive wetting of polydimethylsiloxane as referenced [2,3]. In the sessile drop method (Fig. 1(a)), a millimetric drop is gently deposited on the sample and the drop volume is quasi-statically increased to measure θ_{adv}, and then decreased to measure θ_{rec}. In the tilted plate method (Fig. 1(b)), a millimetric drop is positioned on the surface and the target surface is inclined, the downhill, $\theta_{downhill}$, and uphill, θ_{uphill}, contact angles are

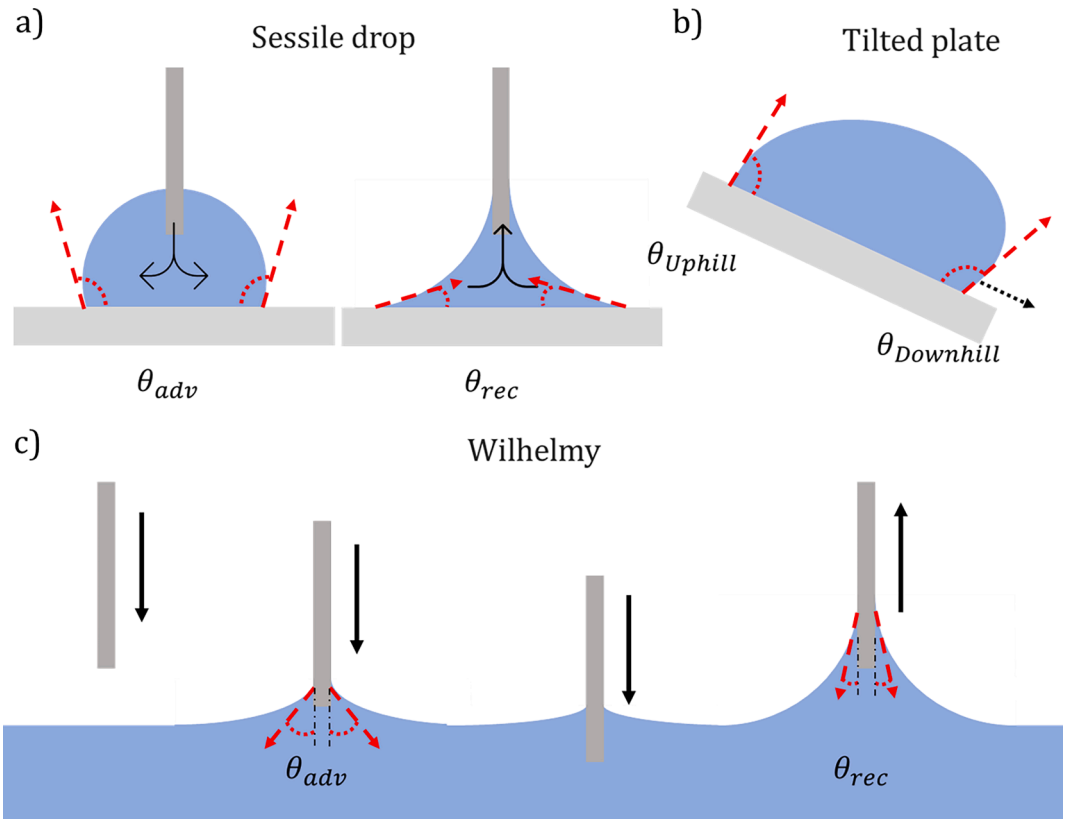

Fig. 1. Schematics of $\Delta\theta$ measurement methods to measure contact angles: (a) sessile drop, (b) tilted plate, and (c) Wilhelmy plate.

measured on opposite sides of the drop as it begins to slide; these values are similar but conceptually different from θ_{adv} and θ_{rec} as highlighted in a careful comparative study in [18]. Nonetheless, many studies use the approximations $\theta_{downhill} \approx \theta_{adv}$ and $\theta_{uphill} \approx \theta_{rec}$ to predict drop adhesion on tilted surfaces. In the Wilhelmy plate method (Fig. 1(c)), the surface is immersed into a liquid pool and carefully withdrawn: θ_{adv} and θ_{rec} are recorded during immersion and withdrawing, respectively. All methods have limitations, and the choice of the measurement method depends on the sample characteristics, and the target application. Moreover, it is revealed that due to the inherent difference in the physical nature of these methods, the results of any particular method are not necessarily applicable to other methods [2,12,18–20]. In sessile drop and tilted plate methods, the drop size becomes a crucial factor due to the influence of gravity on the experiment. The drop Bond number (Bo), defined as $Bo = \rho g l^2/\sigma$, where ρ and σ are density and surface tension of the liquid, g is gravity acceleration, and l is the characteristic length for the liquid (such as the radius of the drop), plays a significant role during measurements. Therefore, comparing wetting experiments within similar ranges of Bond numbers is important. Results obtained with very different Bond numbers using the same method may not be equivalent [12,18,21].

It is worth noting that methods listed here consider the drop in steady motion and cannot track changes in the drop lateral force on the surface once the drop starts to slide [2]. To quantify the kinetic lateral force during sliding, researchers have employed friction force-based methods. Among these methods are studies on the drop dynamics under the influence of a centrifugal force [2], airflow shedding of the liquid from the surface when exposed to aerodynamic forces[18], and force-based techniques based on moving plate experiments with the presence of a deflectable capillary stuck in the drop [14,19,22–24].

Among the above methods, the sessile drop is the most commonly used due to its simplicity [3]. Recent developments in optical imaging and contact line tracking through computational tools enable the use of sessile drop method to provide information not only about extreme contact angles but also about drop evolution on the surface. However, the sessile drop has several limitations affecting its precision, due to the chemical and morphological characteristics of the solid surface like uniformity, heterogeneity, and defects, as well as from the experiment method, and interpretation of the results [25]. Other material properties such as surface elasticity [26], viscoelasticity [27,28], and porosity [1] can also significantly affect the wetting behaviour. The error sources practically can be categorized as following: (i) roughness and heterogeneity, (ii) infusion/withdrawal rate, (iii) disturbance by the needle, and (iv) extreme wetting conditions. First, increased surface roughness and heterogeneity can make reported contact angles drop-size dependent. The use of larger drops can mitigate the influence of surface heterogeneity. For θ_{rec}, proper experiment requires significantly larger drops of volumes near 100 μl or a drop initial diameter larger than 4–5 mm (Bo $>$ 1) [7,12,25]. Second, it is necessary to find an optimal infusion/withdrawal velocity depending on the sample characteristics to provide quasi-static conditions and properly account for the liquid–solid adaptation during experiment [2,27,29–31]. To find the optimal rate, the timescales for surface adaptation and liquid mobility on the surface need to be quantified. Third, the presence of the needle inside the drop introduces disturbances in the drop shape, and this is particularly critical on high hysteresis surfaces [7,29]. Fourth, optical methods are challenging for very low ($<20°$) or high ($>160°$) contact angles, possibly suggesting alternative approaches for accurate measurements at these extremes [3,32–34]. These error sources, together with the lack of an automated and standardized process for extracting θ_{adv} and θ_{rec} from the contact angle evolution curve, particularly on complex surfaces, calls for an objective measurement protocol.

Within the above discussed framework, there is a need to employ a robust tool that minimizes human error interference for the analysis and observation of the liquid wetting process on surfaces. The quality of recorded images is contingent on the imaging equipment used, including the camera, lens, and illumination, alongside any data storage limitations. Given the dynamic nature of this experiment, variations in the three-dimensional shape of the drop on the surface and surface irregularities leading to drop movement introduce fluctuations in focus between different frames of the film. Notably, issues such as changes in focus, image quality, and clarity of drop edges present inherent limitations and challenges in wettability analysis using this method, as already discussed for static contact angle measurements in [35], where an open-source tool, Dropen, was developed. To address these challenges, greater emphasis on accuracy and comprehensiveness during the post-processing of wetting videos using computer software is crucial. Striving for independence from user input as much as possible enhances the potential for a comprehensive, accurate, and consistent review of the videos. This approach allows for meaningful comparisons in the analysis of different videos.

Drop image analysis and contact angle evolution software are available with commercial equipment. In addition, depending on the application, some research groups develop appropriate codes for drop image analysis. There are a few open-source code and software available for use. Among them, DropSnake [36] and LB-ADSA [37] (plug-ins for ImageJ) and OpenDrop [38] are available for the analysis of individual images and image sequences, but not for direct analysis of videos from quasi-static wetting experiments. In commercial software θ_{adv} and θ_{rec} are typically calculated by averaging the contact angle data in user-selected regions on the contact angle vs. time curve during the inflation and deflation of the droplet, respectively. In some commercial instruments, there is an option for automatic determination of θ_{adv} and θ_{rec} by calculating the average of the contact angles in a very short region close to the maximum contact diameter during the inflation or deflation of the droplet, respectively. However, this method lacks an appropriate drop mobility tracking strategy and may encounter large errors when analysing wetting on non-ideal surfaces. Recently, Wood et al. introduced ARCA Finder to analyse the data extracted by SCA20 software available in DataPhysics instruments [39,40]. There are also attempts to measure the contact angle of irregular shaped droplets by optimizing fitting methods, like [41,42].

In this study, we introduce an upgraded version of the Dropen software [35], named DropenVideo, to analyse quasi-static wetting experiment videos for automatic determination of θ_{adv} and θ_{rec}. In DropenVideo, similar to Dropen, three methods including the circle mask, polynomial fitting, and circle fitting are available to determine the contact angle for each frame of the video. DropenVideo demonstrates robustness in tracking the evolution of the contact line during quasi-static contact angle analysis. Notable features in the image analysis section of DropenVideo include a reduced video analysis time achieved by limiting the automatic search area of the contact points. Additionally, the software employs slope tracking at the drop edge to correct potential data defects caused by variations in focus and light illumination during experiment, ensuring the analysis of the maximum number of frame images. In contrast to commercial instruments, DropenVideo does not limit the search region for extreme contact angles and defines three main phases in the contact angle (θ)-contact diameter (D) curve: advancing, transition, and receding phases, providing a comprehensive analysis of the drop contact diameter on the surface. In DropenVideo, three fitting lines are identified in these regions to investigate θ_{adv} and θ_{rec}, with a fully automatic process with no human input required. Finally, DropenVideo is open-source and can be thus further developed by the scientific community.

2. Methodology

2.1. Wetting scenarios on various surfaces

The applicability and the accuracy of the automatic drop video analysis codes including DropenVideo are significantly affected by two

main limitations: (i) imaging quality and its consistency in all the frame images, and (ii) more importantly, the inherent sample characteristics, such as roughness, heterogeneity, porosity, softness, flexibility, and adaptivity. All these properties affect the imaging quality during video recording, and can result an error in the contact angle evolution curve, i.e. the contact angle (θ) – contact diameter (D) curve. In the cases with a drop evolution trend that deviates from the standard curve, the determination strategy of θ_{adv} and θ_{rec} via the contact angle evolution data needs to be defined and practiced for that specific case. Regarding the influence of the imaging parameters in the quality of a single frame image, a comprehensive study has been conducted in the paper dedicated to the introduction of Dropen [35], where a guide for contact angle test imaging protocol is presented and discussed. Here, the specific issues related to the measurement of θ_{adv} and θ_{rec} from the drop evolution video are discussed.

Typically, in a quasi-static wetting experiment, a small drop ($1-2\mu l$, $Bo \ll 1$) is gently deposited on the surface, then liquid is slowly infused into it at a flow rate of $1-10\mu l min^{-1}$. While the drop volume is increasing, the contact angle (θ) grows and the diameter (D) is pinned. When θ_{adv} is reached, the contact line starts moving and continues while liquid is infused into the drop, labelled as 'advancing' phase in Fig. 2(a). To investigate the drop receding motion, the liquid is then withdrawn at low rate ($1-10\mu l min^{-1}$). Initially, as the drop volume decreases the contact area remains constant and the contact angle decreases, the 'transition' phase in Fig. 2(a), until θ_{rec} is reached and the contact line starts receding, corresponding to 'receding' phase in Fig. 2(a) [12,25]. It is common that the drop does not grow symmetrically with respect to the needle, and that in the 2D drop projection image only the left or right contact point moves. If this is the case, then the contact angles should be measured only on one side.

During a quasi-static wetting experiment on an ideal solid surface, typically on smooth, rigid surfaces, θ_{adv} can be easily determined as the average value during the advancing phase in Fig. 2(a), with the contact angle remaining constant and equal to the value measured at incipient motion. Analogously, θ_{rec} is ideally determined during the receding phase [17,25]. However, practically real samples are far from ideal smooth surfaces and a full analysis of the drop evolution on the surface is necessary. First, while it is likely that the contact angle remains constant or approximately constant in the advancing phase, in the receding phase the contact angle may decrease significantly; as such, the strict definition of the contact angle at the point of incipient motion has to be used when defining the receding value. This occurs because the drop contact angle on the surface is a local parameter, exhibiting variations at different points along the contact line, and θ_{rec} is more sensitive to heterogeneities. This behaviour becomes apparent when assessing the durability of superhydrophobic coatings, with data showing that θ_{adv} may not necessarily change on damaged coatings, whereas θ_{rec} can decrease significantly, leading to an increase of $\Delta\theta$ and the drop adhesion on the surface [43]. Consequently, non-ideal smooth surfaces with inherent roughness and heterogeneity cause the liquid to get pinned at certain points along the contact line, leading to nonhomogeneous contact line propagation during quasi-static wetting experiment.

To visually represent the changes in the contact angle evolution curve of the samples with different nature, three sketches of possible contact angle evolution curves are represented in Fig. 2(b)-(d), besides the sketch for ideal solid in Fig. 2(a). In summary, the possible wetting scenarios on various surfaces can be one of the following cases:

(a) on an ideal solid surface (i.e. smooth, homogeneous, inert, and non-deformable), there is a sharp transition between the three phases (advancing, transition, and receding), with constant contact angle values in the advancing and receding phases (Fig. 2(a));

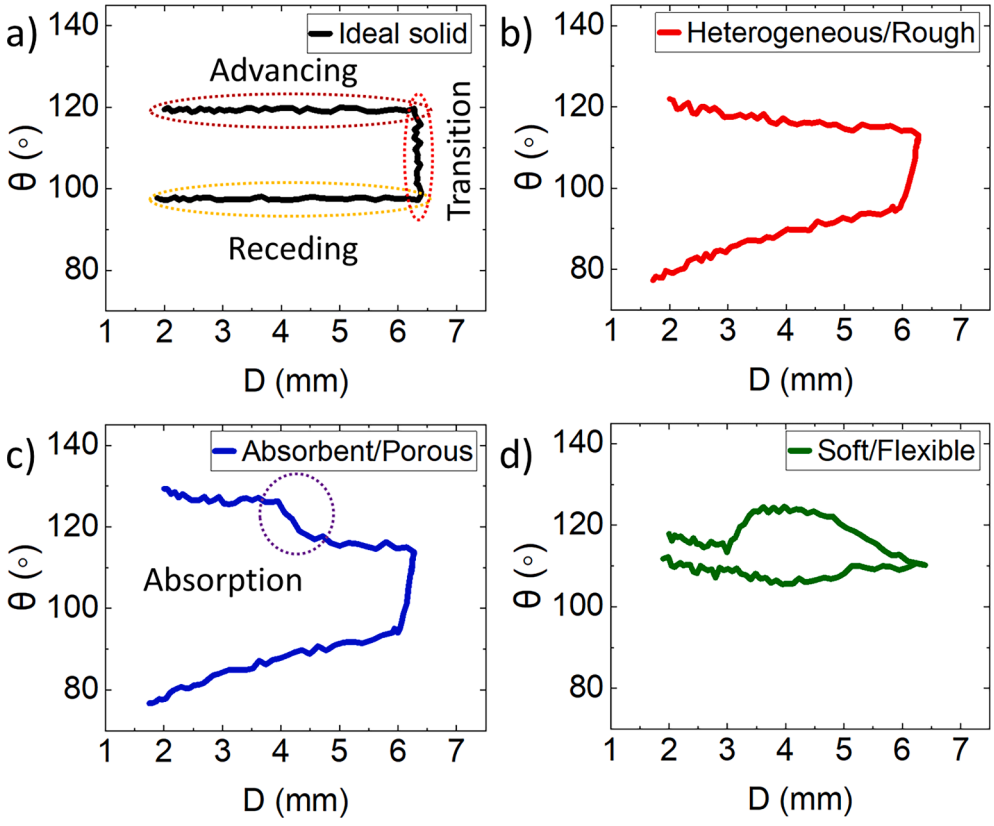

Fig. 2. Sketches of possible contact angle-contact diameter evolution curves in a quasi-static wetting experiment using the sessile drop method, on: (a) ideal smooth, (b) heterogeneous or rough, (c) absorbent or porous-like, and (d) soft or flexible surfaces.

(b) on an heterogeneous and rough surface, composed of patches with different chemical nature or physical structure, and inhomogeneous or non-continuous drop motion on the surface during the experiment. Consequently, the distortion in drop motion on the surfaces causes inclination and eventually stick–slip behaviour, particularly in the receding phase (Fig. 2(b)) [2,44–46].

(c) on an absorbent and porous surface, like membranes, there are multiple stepwise reductions in the advancing phase due to the local absorption of the liquid by the surface underneath, especially in the early moments of the drop infusion (Fig. 2(c)). Depending on the capacity of the surface to absorb the liquid, this could prevent extra absorption during the liquid withdrawal, resulting in no steps in the receding phase, as shown in the sketch in Fig. 2(c), or alternatively in some cases no contact line retraction could happen, corresponding to θ_{rec} close to 0° [47–49].

(d) on soft and flexible surfaces, like elastomers and hydrogels, the unbalanced vertical component of the liquid surface tension can deform the contact surface between the drop and the solid by a distance of order of the elastocapillary length scale, the ratio of the liquid surface tension and the solid Young's modulus (Fig. 2 (d)). This leads to the formation of a wetting ridge at the contact line as well as compression of the material below the drop due to Laplacian pressure within the drop [2,50]. As a result, the hysteresis increases substantially and non-uniformly along the contact line, and the contact angle evolution curve deviates significantly from the standard curve observed in ideal solids. In the case where the surface responds viscoelastically, stick–slip behaviour can be observed, and measurement become time dependent (i.e. dependent on the liquid infusion and withdrawal rate) [27,51].

2.2. Flowchart of DropenVideo

Fig. 3 represents the flowchart of DropenVideo. The flowchart includes three main sections: 'Initialization', 'Iterations', and 'Finalization'. In the 'Initialization' section, the software receives the video, splits it into single frames, and the user defines the window frame to be analysed. To reduce the computational cost and the process time, the user selects the drop region and the baseline in a sample frame of the video. If the baseline is not horizontal, the code rotates all frame images to level the drop. It is important to note that this selected baseline is an initial guess, as the correct baseline will be identified by the software.

In 'Iterations', the main section of the code, an iteration on the frame images is applied to determine the contact points and contact angles at left and right sides of the baseline in each frame. In this section, the needle and the baseline are removed by tracking the changes in intensity gradients on drop edges. In addition, a drop edge refining step is applied to the drop edge data, using polynomial interpolation, if pixels on the drop edge are missing due to low image quality or light illumination bright spots. After all these treatments the drop image is refined and analysed by the previously developed Dropen software for static images [35]. In this step, contact points on the drop left and right sides are identified automatically in a small area around the user defined baseline. In short, in this step the code calculates the local slopes in the drop contour by calculating the overlap area between the drop image and a predefined circle mask, and finds the points on the drop contour with maximum local slope. Then, contact angles are calculated on the drop left and right sides using the circle mask, polynomial and circle fitting methods. In the 'Finalization' section, the contact point positions, contact diameter, and contact angles calculated using three different methods, are collected for all the frame images and refined by removing unsuccessful frames and outliers on the data. To calculate θ_{adv} and θ_{rec}, according to the discussion carried out in Section 2.1 and the sketch in Fig. 2(a), advancing, transition, and receding phases are defined on the contact angle evolution curve by considering the data from the frames

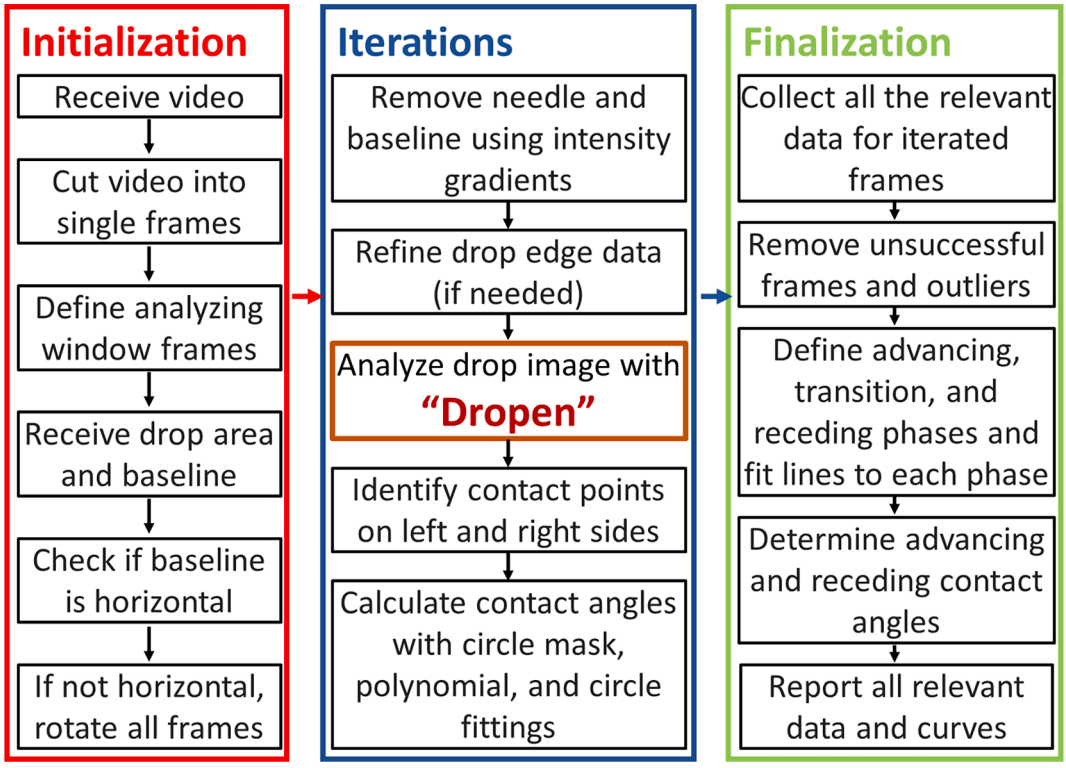

Fig. 3. Flowchart of DropenVideo to analyse the contact angle evolution of a liquid drop on a solid surface during a quasi-static wetting experiment. The flowchart includes three main sections: 'Initialization', 'Iterations', and 'Finalization'.

with contact diameters larger than a minimum contact diameter threshold based on the maximum contact diameter, ($D_{min} \geq 70\% D_{max}$ is the preset option in DropenVideo). These three phases are defined by the following criteria:

1. Advancing phase: if (a) contact diameter is within the range [D_{min}, 95 % D_{max}], and (b) the frame number is smaller than the frame where the contact diameter is maximum;
2. Transition phase: in the rest of the frames, if contact diameter is larger than 95 % D_{max};
3. Receding phase: the rest of the frames until the contact diameter is within the range [D_{min}, 95 % D_{max}].

After three phases are identified, linear data fitting is employed to each phase. θ_{adv} is calculated as the average value in the advancing phase. Half of the difference between the minimum and the maximum θ in the advancing phase is considered as the uncertainty in the determination of θ_{adv}. For θ_{rec}, five fittings are conducted in the transition phase, corresponding to contact diameters ranging from 95 % to 99 % of D_{max}. Then, intersections between each of these five lines and the fitted line to the receding phase are calculated as possible receding contact angles. From these, the intersection with minimum regression in the fitting to the transition phase is selected as the final θ_{rec}. The error in θ_{rec} is calculated from the maximum difference between those five intersections and the selected θ_{rec}. Clearly the user must conduct multiple quasi-static wetting experiments to collect adequate statistics and ensure test repeatability.

DropenVideo provides comprehensive data, including contact positions, contact diameters and contact angles, and plotted curves. This allows users to dynamically recalculate θ_{adv} and θ_{rec} based on the specific characteristics of the examined sample. Users can customize various parameters in DropenVideo, including: (i) image contrast threshold; (ii) starting and ending frames along with timesteps for analysis; (iii) toggle for applying edge data refinement;(iv) method for contact angle determination (circle mask, polynomial, and circle fittings); (v) width of the scanning area to refine the user-selected baseline; and (vi) chosen region in the contact angle evolution curve for exploring θ_{adv} and θ_{rec}. All the contact angle data shown in the present paper have been obtained using the circle fitting method.

3. Results

To ensure robustness and to validate DropenVideo, fifteen example videos from real experiments featuring various imaging qualities and surface characteristics were gathered from researchers in the field. In the following, first the analysis of an example video (V1) with good resolution and contrast by DropenVideo is presented. Subsequently, a comprehensive discussion on the potential error sources in the drop imaging, and determination of θ_{adv} and θ_{rec} has been carried out using videos over a wide range of experimental conditions (V2–V12). Even-

Table 1
Details of the selected example videos V1–V15 in this study, together with an overview of challenges and limitations encountered in processing quasi-static wetting experiments by DropenVideo.

Video	Film/ substrate	Hard/ soft layer	Image size (px.)	Max. drop size (µl)	Bond n.	N. processed frames	N. modified frames	N. failed frames	Analysis limitation	θ_{adv} (°)	θ_{rec} (°)	Elapsed analysis time (s)
V1	Bitumen on glass	Hard	600 × 500	7	0.189	600	0	0	–	106 ± 1	80 ± 1	33
V2	PDMS on glass	Soft	700 × 500	8	0.206	292	0	0	Inclined advancing phase	108 ± 3	84 ± 1	20
V3	PDMS on glass	Soft	600 × 500	8	0.206	289	21	1	Not clear baseline	108 ± 4	83 ± 2	37
V4	FDTS on Si	Hard	500 × 400	17	0.341	442	0	12	Low quality imaging	107 ± 1	91 ± 1	20
V5	Cu on Au/ Si	Hard	500 × 400	8	0.206	797	9	31	Very short transition phase due to superhydrophobicity	144 ± 1	138 ± 1	50
V6	MTS on glass	Hard	500 × 500	8	0.206	329	7	0	Very high illumination, disrupted contact area, very low hysteresis	138 ± 1	137 ± 1	23
V7	Cu on steel mesh	Hard	500 × 500	8	0.206	735	187	2	Rough mesh surface, liquid moving between the mesh wires	–	–	37
V8	PTFE on glass	Hard	1000 × 500	170	1.583	2953	2667	26	Dust in contact area	99 ± 3	79 ± 2	273
V9	PDMS on glass	Soft	350 × 250	8	0.206	1090	75	2	–	116 ± 1	75 ± 1	76
V10	PDMS on glass	Soft	350 × 250	8	0.206	1961	8	1	Small or not reached receding phase	112 ± 1	88 ± 2	123
V11	MTS on glass	Hard	350 × 250	8	0.206	664	0	66	Not reached or very low receding phase	96 ± 2	–	31
V12	MTS on glass	hard	1000 × 700	8	0.206	353	64	290	Moving drop on the surface-losing focus during experiment	–	–	226
V13	Chitosan hydrogel	soft	350 × 250	8	0.206	862	239	62	–	–	–	62
V14	PDMS on glass	soft	1000 × 500	170	1.583	32,851	1965	7697	–	–	–	2702
V15	PVC on glass	Hard	1000 × 500	170	1.583	33,705	9	1726	–	–	–	2924

tually, in the next section, V13–V15 are presented for the studies on the drop contact line mobility on the surface. The details of imaging and analysis of the example videos V1–V15 are summarized in Table 1. Table 1 includes information on the sample characteristics, the imaging features, the number of analysed frames, the number of frame images modified by the code to facilitate analysis, the number of frames where the code encountered failures, along with an explanation of the causes behind those failures, the determined θ_{adv} and θ_{rec}, and the elapsed time for the analysis of the video by DropenVideo. The elapsed time of the analysis depends on various factors, including the computer specifications, the image size, the number of processed frames, and the number of frames with the edge refinement. In the results shown in this paper, analysis was conducted using a laptop equipped with an AMD Ryzen 5 PRO 4650U processor clocked at 2.1 GHz, boasting 6 cores, and bolstered by 16 GB of RAM. Based on Table 1, DropenVideo analyses every 100 frames within 5 s in videos featuring an image size of 500 × 500*px*. , with no necessity for drop edge refinement. V1 together with a video recorded from the screen during analysis of V1 by DropenVideo are available as supplemental videos, see Appendix A. High quality V1–V15 videos are available at BOA, the Bicocca Open Access public repository, see Appendix A.

3.1. Good practices

Fig. 4(a)–(c) illustrate selected frame images from the quasi-static contact angle measurement on a smooth and hard bitumen coating on a glass substrate (V1) [27] corresponding to the initial, maximum drop volume, and the final frames, see Table 1 for details on the imaging and analysing by DropenVideo. From Fig. 4(a)–(c) and Table 1, the imaging quality remains consistent during video recording, facilitating the analysis of all frame images by the code and improving the accuracy of contact angle determination. After analysing 600 frames, acquired at a frame rate of 12 fps (corresponding to a 50 s video), the contact angle and drop contact diameter reveals a smooth evolution between the infusion and the withdrawal steps of the liquid on the sample, see Fig. 4 (d) and (e). These gradual changes result in an almost standard contact angle evolution curve in Fig. 4(f), featuring a constant contact angle during the liquid infusion in the advancing phase, followed by a transition phase and a distinct change to the receding phase. The resulting θ_{adv} and θ_{rec} are $106^{\circ} \pm 1^{\circ}$ and $80^{\circ} \pm 1^{\circ}$, respectively.

3.2. Challenging measurements

The limitations in analysing quasi-static wetting experiments are illustrated in example videos V2–V12 and summarized in Table 1. The corresponding contact angle evolution curves are shown in Fig. 5.

V2 (Fig. 5(a), details in Table 1) is an example of a soft surface with characteristics deviating from the ideal smooth solid surface, with good imaging quality. The analysis of V2 by DropenVideo is successful for several reasons: (i) the number of available pixels on the drop edge are high, significantly enhancing the accuracy of automatic determination of the contact point positions and contact angles by DropenVideo; (ii) the image effectively presents a good contrast between the liquid and the environment; (iii) the focus remains sharp throughout the drop spreading and retraction on the surface, minimizing the risk of analysis failure; (iv) thanks to the quality of imaging, the analysis process is fast, with 292 frames analysed in 20 s; (v) despite the surface is far from the ideal solid surface, the contact angle evolution curve aligns with the protocol introduced in section 2; (vi) consequently, the reported θ_{adv} and θ_{rec} by DropenVideo demonstrate a very low error. The $\pm 3^{\circ}$ error in the determination of θ_{adv} is due to a slightly decreasing contact angle during the advancing phase.

V3 represents a similar sample and imaging characteristics with V2, but with a diffused and unclear baseline position, see the inset in Fig. 5 (b). Consequently, the analysis time extended to 37 s, an indication that extensive image analysis is required for modifying the drop edge data in 21 frames. Additionally, the error in the determined extreme contact angles increased to $\pm 4^{\circ}$, see Table 1.

V4 is an example of a recorded video that lacks precision in the image quality and optimal light exposure, see the inset in Fig. 5(c). Despite sub-optimal contrast and transparency in the video, the automatic code identifies the drop edges in most of frames, encountering only 12 failures out of 442 frames, see Table 1. The video analysis, completed in 20 s, yields an almost standard contact angle evolution curve with some outliers.

V5 shed lights into the challenge of determining θ_{adv} and θ_{rec} on

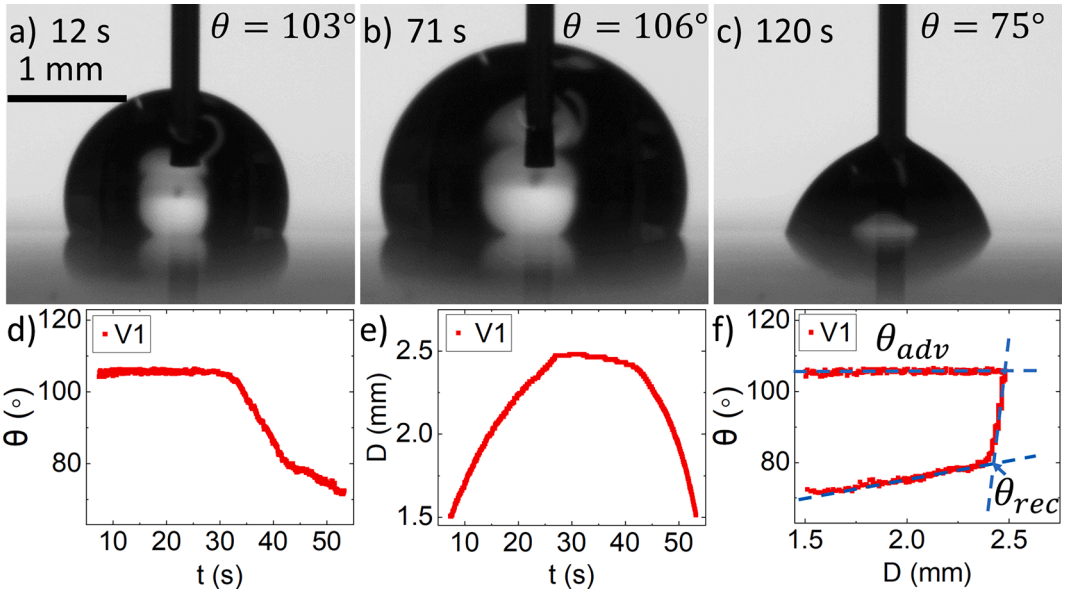

Fig. 4. The quasi-static wetting experiment on smooth and hard bitumen coating on glass substrate (V1) analysed by DropenVideo: (a)–(c) images from the initial, maximum drop volume, and one of the final frames of the recorded video, all within an imaging window of size 600 × 500*px*., resolution of $7.8 \mu m px^{-1}$, and infusion rate of $6 \mu l min^{-1}$. The resulting (d) contact angle calculated from circle fitting vs. time, (e) drop contact diameter on the surface vs. time, and f) contact angle vs. drop contact diameter, i.e. contact angle evolution curve, with fitted lines representing the advancing, transition, and receding phases are presented. θ_{adv} and θ_{rec} are marked on the curve in (f).

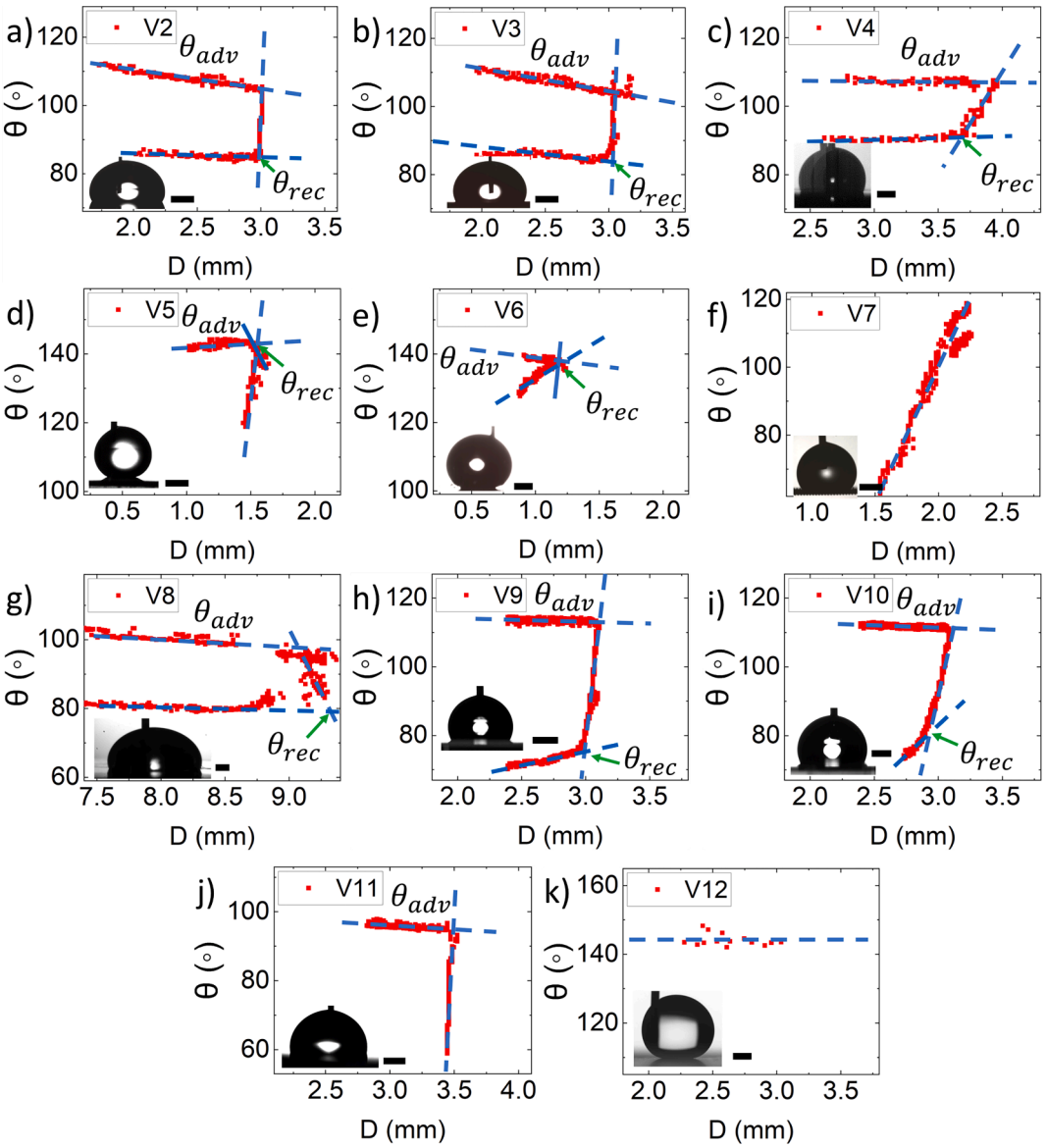

Fig. 5. Contact angle evolution curves of V2–V12 videos plus an example frame image of each video as an inset. The length of horizontal as well as vertical axis are identical in all curves. The determined θ_{adv} and θ_{rec} are marked on each curve. The black solid line beside the example frame images corresponds to 1 mm scale.

superhydrophobic surfaces. The contact angle evolution curve indicates on a short transition phase between the advancing and receding phases, posing a challenge for utilizing the fitting lines to the phases, see Fig. 5 (d). Nevertheless, DropenVideo provides both the analysis data and the contact angle evolution curve, enabling users to easily determine the extreme angles. The highly curved drop shape in contact with the superhydrophobic surfaces cause another challenge during measuring the contact angle by conventional fitting equations as well as the convolution methods like the circle mask used in DropenVideo. Consequently, there is a risk of underestimating the contact angle, as discussed in detail in the paper on Dropen [35].

V6 represents a superhydrophobic sample, similar to V5, but with an oversaturation of light illumination during imaging, see inset in Fig. 5 (e). Although a more intense backlight illumination can enhance the contrast close to the surface, the risk is that the edge appears diffused, and the contact angle values are scattered, as visible in the curve depicted in Fig. 5(e) and the details presented in Table 1.

V7 highlights the challenge posed by highly rough surfaces. The sample was a stainless steel mesh (opening diameter = 80 μm, wire thickness = 50 μm) covered by a hydrophobic Cu layer. Due to a large porosity, the contact line 'jumps' or 'slides' when overcoming to the subsequent mesh wire, causing semi-linear increase/decrease in the contact diameter, as evident in the contact angle evolution curve in Fig. 5(f). Consequently, the standard protocol is not applicable for cases like V7. An additional challenge arises in the analysis of highly rough and porous samples using software like DropenVideo, attributes to the presence of surface prominences like mesh wires. In many cases, the automatic image analysis functions cannot differentiate between the drop curvature and the surface grooves. Consequently, the number of failed frames may increase, or alternatively, the baseline must be selected above the level of the surface grooves, introducing a potential error source to the resulted data [35,52].

V8 represents an example of a video recorded with high resolution and imaging quality, however the measurement is jeopardized by the presence of a dust fiber near the three-phase contact point, see Fig. 5(g). This presence of dust disrupts the edge detection function of the code in the right side of the drop across all frame images. As indicated in Table 1, the code reconstructs the edge data in the right side using polynomial extrapolation, displaying a minor deviation from the actual drop edge, depending on the sample characteristics. Nonetheless, DropenVideo can

analyse V8, providing output values for θ_{adv} and θ_{rec}. Here the user needs to critically examine at the results and decide if the measurement can be used, or, more likely, whether other tests without dust should be repeated to ensure that the measured contact angle values are representative of the surface and not affected by the dust. The elapsed time for V8 video analysis was $4.5min$, significantly longer than other samples, owing to the considerably larger image size and the necessity of drop edge refinement in around 1000 frames.

V9 and V10 exhibits the quasi-static wetting experiment on similar soft samples with distinct surface modifications. The imaging quality is high in both videos and the code successfully analysed the videos, see Table 1 and Fig. 5(h) and (i). In V9, the receding phase is reached during the video recording, allowing the standard protocol to be applicable to the contact angle evolution curve. In V10, although the code identifies θ_{rec} following the standard protocol, θ_{rec} rapidly reduces in the receding phase: it would be advisable to repeat the test at a lower withdrawal rate.

V11 represents the results on a chlorosilane coated glass slide. In this example video, the user stopped the video recording before the drop began receding on the surface. This error by the user renders the standard protocol inapplicable for determining θ_{rec}, see Table 1 and Fig. 5(j).

V12 is an example of an incorrect focus setting during video recording. In this case, the lens is focused on the needle rather than the drop, as well as the drop is sliding on the sample during recording, see Fig. 5(k). Consequently, in a few certain frame images, DropenVideo successfully identifies a larger part of the drop edge and refines the edge data accordingly, see Table 1. However, in most of frames, the edge remains unclear to the edge detection functions of the code. This case highlights the requirement of high-quality videos, with sufficient resolution and drop correctly in focus, with homogeneous illumination.

In addition, a comparison with the manual determination of θ_{adv} and θ_{rec} in three example videos presented in this study (V1, V5, and V9) and the results from DropenVideo are discussed in detail in the Supporting Information. For video V1, manually selecting the frame with the maximum contact diameter and the receding frame resulted in a low error. However, for the more hydrophobic cases (V5 and V9), these identifications were challenging. The user error was much higher in identifying the receding frame in these two latter videos, with most users unable to identify the receding frame in the superhydrophobic sample, V5. After comparing the contact angles in the frames selected by the users and analysed by DropSnake in ImageJ with the data determined by DropenVideo, it is concluded that while the error in calculated θ_{adv} is smaller than 10°, the error in θ_{rec} shows a much larger difference from the automatic DropenVideo. This confirms the influence of inaccurate and biased determination of the receding frame by humans.

3.3. Additional examples of wetting studies

As discussed in the introduction, defining the wetting state of a surface only by its extreme contact angles is not enough to understand the wetting characteristics of surfaces and their relevance for real-world applications especially for more dynamic and interactive surfaces. Therefore, there is a need for an in-depth dynamic analysis of liquid evolution on the surface. DropenVideo is already efficient and reliable in analysing images and tracking liquid movements on surfaces during wetting experiments. The extended mission for this software is to enhance its capabilities to create a more powerful and versatile software for diverse fluid mechanics studies. As such, the extended applications for DropenVideo could include analysing how drops move on surfaces during impact experiments (contact line motion) and tracking liquids in microfluidic channels. In the following, three detailed examples from ongoing studies by DropenVideo on the movement of the contact line are provided.

Fig. 6(a) illustrates an example of tracking drop dynamics on a soft absorbent chitosan electrolyte hydrogel surface (V13)[53] using DropenVideo. In Fig. 6(a1), multiple steps of liquid absorption and its stick–slip sliding on the surface during the advancing phase are observed, until a thin layer of water forms beneath the drop. Subsequently, during the receding phase, the drop initiates to retract from the surface, which is evident from the rapid decrease in contact angle shown in Fig. 6(a2), while the contact diameter remains constant for $t > 100s$. The contact line mobility curve in Fig. 6(a3) confirms that the contact line mobility becomes almost constant and close to zero after $100s$ of the experiment.

Two examples of wetting over much longer timescales for larger drops (resulting in higher Bond numbers) and higher contact line velocities are shown in Fig. 6(b) and (c). These sample videos, V14 and V15, depict multiple cycles of a water drop being infused and withdrawn on PDMS and PVC surfaces, respectively, with a 60-second pause between each advancing and receding stage. For these cases, the infusion/withdrawal flow rate was $1200\mu lmin^{-1}$, resulting in high contact line velocities ($1mms^{-1}$). In Fig. 6(c2), for the PVC (V15), there is a single advancing contact angle during infusion, followed by a rapid decrease in contact angle while the drop remains pinned during the initial part of the withdrawal stage (see Fig. 6(c1) and (c3)). Therefore, unlike studies with low contact line velocities, there is not a single receding contact angle value when the contact line starts to move [31]. Instead, the contact angle slightly decreases with the drop diameter and then sharply decreases to a minimum value. This is followed by a significant increase in contact angle from 45° to 60° during the final period of the withdrawal stage. These observations are similar to those by Wong et al. [31] on PDMS at a flow rate of $120\mu lmin^{-1}$. For the PDMS case (V14), shown in Fig. 6(b), a similar but less pronounced minimum peak is observed (Fig. 6(b2)), with much greater hysteresis (Fig. 6(b1) and 6(b3)). Fig. 6 (d) displays the contact angle evolution curves of both V14 and V15 in a single plot, facilitating the comparison of high contact-line velocity wetting on these polymers.

As future development, we envision a potential application of DropenVideo for automatically tracking the contact line motion of drops during impact experiments. These experiments study the behaviour of a liquid drop after it impacts a solid surface from a certain height, examining the interactions between kinetic, adhesion, and friction forces. By tracking the local deformations at the drop edges during and after the impact, we can better understand solid–liquid interactions. Examples of drop behaviour after impacting a highly porous surface can be found in [54]. The development of drop impact video analysis within the DropenVideo software is underway, aiming to provide a simpler and more accurate method for interpreting these experiments compared to manual analysis.

4. Conclusions

DropenVideo, an open-source software, is presented here to enhance the capabilities of Dropen [35] in analysing videos of quasi-static contact angle measurements. By examining fifteen representative sample videos from wetting experiments on complex surfaces using DropenVideo, various wetting scenarios are discussed. DropenVideo facilitates the automated determination of advancing and receding contact angles, and drop mobility on the surface, typically within less than one minute. By tracking the evolution of water drops on solid surfaces, DropenVideo reveals the complexities of interpreting wetting experiments, especially on surfaces with diverse characteristics such as roughness, softness, porosity, heterogeneity, flexibility, and adaptivity [1,7,12]. These findings highlight the importance of employing a user-independent and reliable automatic software for frame-by-frame analysis of wetting evolution videos to mitigate subjective bias inherent in manual interpretation and improve accuracy and precision. Notably, the determination of advancing and receding contact angles is particularly challenging on complex surfaces, underscoring the need to automate and standardize this process [16,17].

In particular, DropenVideo has been designed to introduce an open-

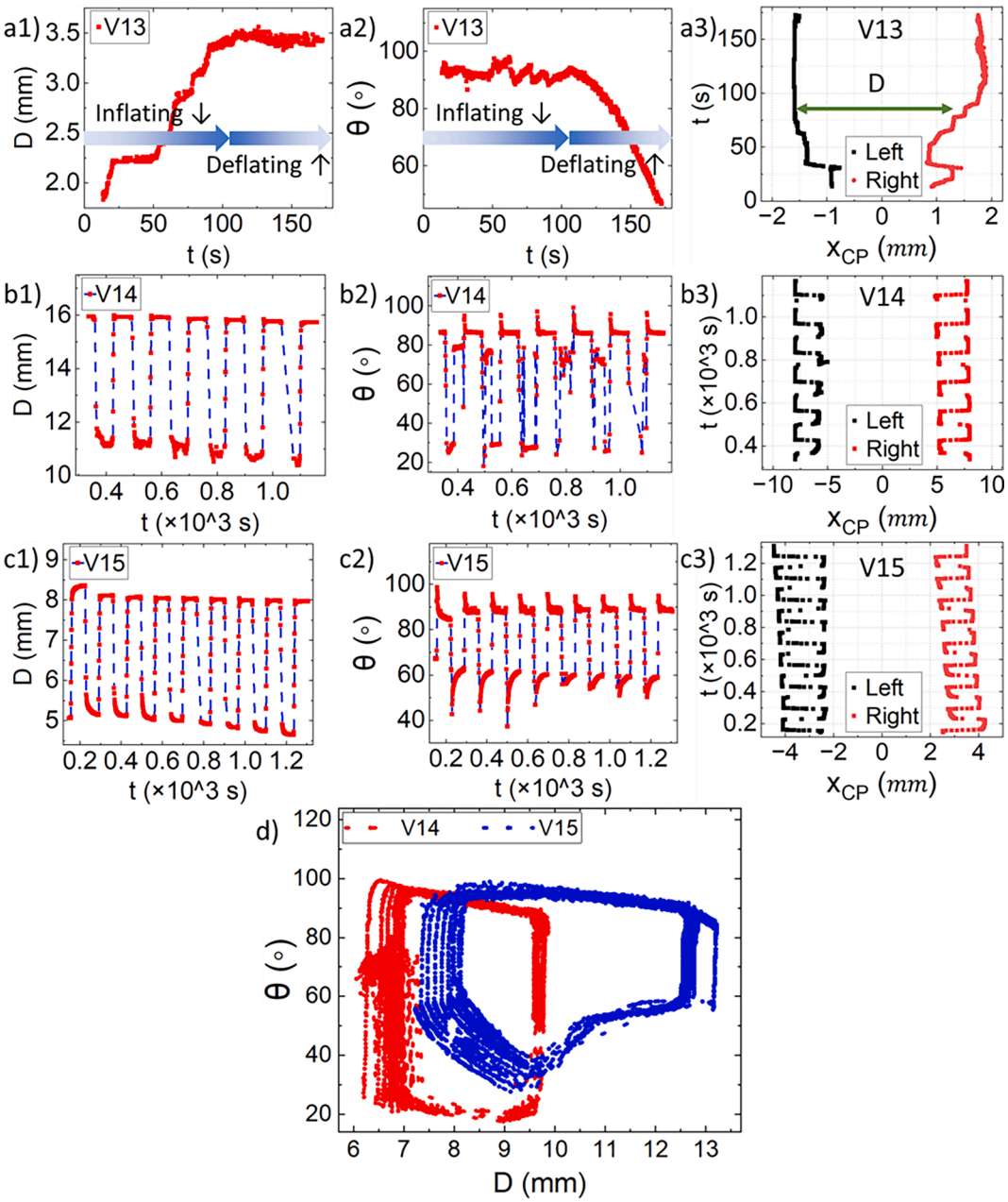

Fig. 6. Tracking (a) the liquid absorption stages on a soft absorbent chitosan hydrogel surface (V13), and wetting during multiple infusion/withdrawal cycles on (b) PDMS (V14) and (c) PVC (V15) layers on glass slide by DropenVideo, see Table 1 for details. (a1),(b1), and (c1) show contact diameter vs. time, (a2),(b2), and (c2) show contact angle vs. time, and (a3),(b3), and (c3) show contact line mobility in left and right sides of the drop, x_{CP}, vs. time. The inflating and deflating of the sessile drop on the surface are represented in (a1) and (a2). (d) Contact angle evolution curves of V14 (PDMS) and V15 (PVC) videos, where multiple injection/withdrawal cycles were conducted.

source, fully automatic tool for analysing quasi-static wetting experiment videos and determining advancing and receding contact angles through a standardized approach, which are pivotal features for surface wetting characterization. These features are notably absent in currently available software. For instance, while commercial software can be used for analysing drop images and videos, the user must manually identify the suitable data points to calculate the advancing and receding contact angles. Although automatic identification is available in some of these commercial instruments, this feature does not follow an appropriate automated strategy to track drop evolution on the surface and identify the advancing and receding regions in the contact angle data. This can result in large errors, especially in studying the wettability of non-ideal surfaces. Recently, ARCA Finder [39,40] has been introduced to determine these contact angles from data extracted from DataPhysics instruments, but it still lacks the full automation developed in this study. Some codes developed by research groups are available for analysing drop images, but few are published publicly and free-of-charge. Notable examples include DropSnake [36] and LB-ADSA [37], plugins in ImageJ, and OpenDrop [38]. However, none of these options offer capabilities for analysing videos.

Key improvements and innovations in DropenVideo include: (i) an increased number of analysed frames in videos with lower imaging quality or disrupted drop edges, through modifications in image contrast and refining missing drop edge data through extrapolation; (ii) options for users to adjust all analysis parameters within the software, including selecting the contact angle calculation method (i.e. convolution mask, circle, and polynomial fittings), and choosing the region in the contact angle evolution curve to extract the advancing and receding contact

angles; and (iii) the automatic identification of advancing and receding contact angles from the contact angle-contact diameter curve, by identifying three phases of drop evolution (advancing, transition, and receding) and optimizing the fitting regression for each phase.

As a future perspective, an upgraded version of DropenVideo will facilitate a comprehensive dynamic analysis of liquid evolution on surfaces, encompassing intricate studies such as drop impact analysis.

CRediT authorship contribution statement

Raziyeh Akbari: Writing – original draft, Visualization, Validation, Software, Methodology, Investigation, Funding acquisition, Formal analysis, Data curation. **Federico Ambrosio:** Software, Investigation. **Joseph D. Berry:** Writing – review & editing, Investigation, Formal analysis. **Carlo Antonini:** Writing – review & editing, Supervision, Project administration, Funding acquisition, Conceptualization.

Declaration of competing interest

The authors declare that they have no known competing financial interests or personal relationships that could have appeared to influence the work reported in this paper.

Data availability

High quality V1–V15 videos and DropenVideo software are available free-of-charge at BOA, the Bicocca Open Access public repository: https://doi.org/10.17632/wzchzbm58p.

Acknowledgements

RA and CA gratefully acknowledge support through a post-doctoral fellowship from the University of Milano-Bicocca, Italy. JDB is the recipient of an Australian Research Council Future Fellowship (FT220100319) funded by the Australian Government. The Authors also extend their sincere gratitude to Anny Catalina Ospina Patino and Veronica Radice for generously providing contact angle evolution videos.

Appendix A. Supplementary material

A Supporting Information text file is available providing information on comparison between the manual determination of the advancing and receding contact angles, with the automatic DropenVideo software. Two supplementary videos, one featuring V1 and another recorded from the screen during the analysis of V1 by DropenVideo, can be found in the online version of the article. Supplementary data to this article can be found online at https://doi.org/10.1016/j.jcis.2048.08.159.

References

[1] J.W. Drelich, L. Boinovich, E. Chibowski, C. Della Volpe, L. Hołysz, A. Marmur, S. Siboni, Contact angles: history of over 200 years of open questions, Surf. Innov. 8 (2020) 3–27, https://doi.org/10.1680/jsuin.19.00007.
[2] H.J. Butt, J. Liu, K. Koynov, B. Straub, C. Hinduja, I. Roismann, R. Berger, X. Li, D. Vollmer, W. Steffen, M. Kappl, Contact angle hysteresis, Curr. Opin. Colloid Interface Sci. 59 (2022) 101574, https://doi.org/10.1016/j.cocis.2022.101574.
[3] H.B. Eral, D.J.C.M. 'T Mannetje, J.M. Oh, Contact angle hysteresis: a review of fundamentals and applications, Colloid Polym. Sci. 291 (2013) 247–260, https://doi.org/10.1007/s00396-012-2796-6.
[4] P. Brunet, J. Eggers, R.D. Deegan, Vibration-induced climbing of drops, Phys. Rev. Lett. 99 (2007) 144501, https://doi.org/10.1103/PhysRevLett.99.144501.
[5] A. Ahmed, R. Sanedrin, T. Willers, P.R. Waghmare, The effect of dynamic wetting pressure on contact angle measurements, J. Colloid Interface Sci. 608 (2022) 1086–1093, https://doi.org/10.1016/j.jcis.2021.10.003.
[6] B.K. Cheng, B. Naccarato, K.J. Kim, A. Kumar, Theoretical consideration of contact angle hysteresis using surface-energy-minimization methods, Int. J. Heat Mass Transf. 102 (2016) 154–161, https://doi.org/10.1016/j.ijheatmasstransfer.2016.06.014.
[7] J. Drelich, Guidelines to measurements of reproducible contact angles using a sessile-drop technique, Surf. Innov. 1 (2013) 248–254, https://doi.org/10.1680/si.13.00010.
[8] W. Choi, A. Tuteja, J.M. Mabry, R.E. Cohen, G.H. McKinley, A modified Cassie-Baxter relationship to explain contact angle hysteresis and anisotropy on non-wetting textured surfaces, J. Colloid Interface Sci. 339 (2009) 208–216, https://doi.org/10.1016/j.jcis.2009.07.027.
[9] C.W. Extrand, A thermodynamic model for contact angle hysteresis, J. Colloid Interface Sci. 207 (1998) 11–19, https://doi.org/10.1006/jcis.1998.5743.
[10] L. Makkonen, A thermodynamic model of contact angle hysteresis, J. Chem. Phys. 147 (2017) 064703, https://doi.org/10.1063/1.4996912.
[11] A. Marmur, Thermodynamic aspects of contact angle hysteresis, Adv. Colloid Interface Sci. 50 (1994) 121–141, https://doi.org/10.1016/0001-8686(94)80028-6.
[12] J.T. Korhonen, T. Huhtamäki, O. Ikkala, R.H.A. Ras, Reliable measurement of the receding contact angle, Langmuir 29 (2013) 3858–3863, https://doi.org/10.1021/la400009m.
[13] D. Daniel, X.Q. Koh, Droplet detachment force and its relation to Young-Dupre adhesion, Soft Matter 19 (2023) 8434–8439, https://doi.org/10.1039/d3sm01178j.
[14] G. McHale, N. Gao, G.G. Wells, H. Barrio-Zhang, R. Ledesma-Aguilar, Friction Coefficients for droplets on solids: the liquid−solid amontons laws, Langmuir 38 (2022) 4425–4433, https://doi.org/10.1021/acs.langmuir.2c00178.
[15] A. Marmur, The contact angle hysteresis puzzle, Colloids Interfaces 6 (2022) 39, https://doi.org/10.3390/colloids6030039.
[16] J.F. Joanny, P.G. De Gennes, A model for contact angle hysteresis, J. Chem. Phys. 81 (1984) 552–562, https://doi.org/10.1063/1.447337.
[17] J.W. Drelich, Contact angles: from past mistakes to new developments through liquid-solid adhesion measurements, Adv. Colloid Interface Sci. 267 (2019) 1–14, https://doi.org/10.1016/j.cis.2019.02.002.
[18] A.J.B. Milne, A. Amirfazli, Drop shedding by shear flow for hydrophilic to superhydrophobic surfaces, Langmuir 25 (2009) 14155–14164, https://doi.org/10.1021/la901737y.
[19] C. Antonini, F.J. Carmona, E. Pierce, M. Marengo, A. Amirfazli, General methodology for evaluating the adhesion force of drops and bubbles on solid surfaces, Langmuir 25 (2009) 6143–6154, https://doi.org/10.1021/la804099z.
[20] S. Sarkar, T. Roy, A. Roy, S. Moitra, R. Ganguly, C.M. Megaridis, Revisiting the supplementary relationship of dynamic contact angles measured by sessile-droplet and captive-bubble methods: role of surface roughness, J. Colloid Interface Sci. 581 (2021) 690–697, https://doi.org/10.1016/j.jcis.2020.07.098.
[21] J. Yang, X. Ma, L. Fei, X. Zhang, K.H. Luo, S. Shuai, Effects of hysteresis window on contact angle hysteresis behaviour at large Bond number, J. Colloid Interface Sci. 566 (2020) 327–337, https://doi.org/10.1016/j.jcis.2020.01.042.
[22] N. Gao, F. Geyer, D.W. Pilat, S. Wooh, D. Vollmer, H.J. Butt, R. Berger, How drops start sliding over solid surfaces, Nat. Phys. 14 (2018) 191–196, https://doi.org/10.1038/nphys4305.
[23] P. Papadopoulos, B. El Pinchasik, M. Tress, D. Vollmer, M. Kappl, H.J. Butt, Wetting of soft superhydrophobic micropillar arrays, Soft Matter 14 (2018) 7429–7434, https://doi.org/10.1039/c8sm01333k.
[24] D. Feldmann, B. El Pinchasik, How droplets move on surfaces with directional chemical heterogeneities, J. Phys. Chem. Lett. 12 (2021) 11703–11709, https://doi.org/10.1021/acs.jpclett.1c03423.
[25] T. Huhtamäki, X. Tian, J.T. Korhonen, R.H.A. Ras, Surface-wetting characterization using contact-angle measurements, Nat. Protoc. 13 (2018) 1521–1538, https://doi.org/10.1038/s41596-018-0003-z.
[26] L. Chen, E. Bonaccurso, T. Gambaryan-Roisman, V. Starov, N. Koursari, Y. Zhao, Static and dynamic wetting of soft substrates, Curr. Opin. Colloid Interface Sci. 36 (2018) 46–57, https://doi.org/10.1016/j.cocis.2017.12.001.
[27] J.B. Lee, S. Dos Santos, C. Antonini, Water touch-and-bounce from a soft viscoelastic substrate: wetting, dewetting, and rebound on bitumen, Langmuir 32 (2016) 8245–8254, https://doi.org/10.1021/acs.langmuir.6b01796.
[28] C. Ospina, P.F. Ibá, I. Tagliaro, L. Stendardo, S. Tosatti, C. Antonini, Low ice adhesion on soft surfaces: elasticity or lubrication effects? J. Colloid Interface Sci. (2024) https://doi.org/10.1016/j.jcis.2024.07.110.
[29] H.-J. Butt, R. Berger, W. Steffen, D. Vollmer, S.A.L. Weber, Adaptive wetting-adaptation in wetting, Langmuir 34 (2018) 11292–11304, https://doi.org/10.1021/acs.langmuir.8b01783.
[30] M.F. Ismail, B. Khorshidi, M. Sadrzadeh, New insights into the prediction of adaptive wetting of a solid surface under a liquid medium, Appl. Surf. Sci. 532 (2020) 147444, https://doi.org/10.1016/j.apsusc.2020.147444.
[31] W.S.Y. Wong, L. Hauer, A. Naga, A. Kaltbeitzel, P. Baumli, R. Berger, M. D'Acunzi, D. Vollmer, H.J. Butt, Adaptive wetting of polydimethylsiloxane, Langmuir 36 (2020) 7236–7245, https://doi.org/10.1021/acs.langmuir.0c00538.
[32] L. Hou, X. Yang, J. Qi, R. Miao, Optical measurements of dynamic wetting and dynamic contact angle, Appl. Opt. 57 (2018) 2597, https://doi.org/10.1364/ao.57.002597.
[33] K. Liu, M. Vuckovac, M. Latikka, R.H.A. Ras, Improving surface-wetting characterization, Science (80-) 363 (2019) 1147–1148, https://doi.org/10.1126/science.aav5388.
[34] A. Mascini, V. Cnudde, T. Bultreys, Event-based contact angle measurements inside porous media using time-resolved micro-computed tomography, J. Colloid Interface Sci. 572 (2020) 354–363, https://doi.org/10.1016/j.jcis.2020.03.099.
[35] R. Akbari, C. Antonini, Contact angle measurements: from existing methods to an open-source tool, Adv. Colloid Interface Sci. 294 (2021) 102470, https://doi.org/10.1016/J.CIS.2021.102470.

[36] A.F. Stalder, G. Kulik, D. Sage, L. Barbieri, P. Hoffmann, A snake-based approach to accurate determination of both contact points and contact angles, Colloids Surf. A: Physicochem. Eng. Asp. 286 (2006) 92–103, https://doi.org/10.1016/j.colsurfa.2006.03.008.
[37] A.F. Stalder, T. Melchior, M. Müller, D. Sage, T. Blu, M. Unser, Low-bond axisymmetric drop shape analysis for surface tension and contact angle measurements of sessile drops, Colloids Surf. A: Physicochem. Eng. Asp. 364 (2010) 72–81, https://doi.org/10.1016/j.colsurfa.2010.04.040.
[38] E. Huang, A. Skoufis, T. Denning, J. Qi, R. Dagastine, R. Tabor, J. Berry, OpenDrop: open-source software for pendant drop tensiometry and contact angle measurements, J. Open Source Softw. 6 (2021) 2604, https://doi.org/10.21105/joss.02604.
[39] M.J. Wood, D.G.K. Aboud, G. Zeppetelli, M.B. Asadi, A.M. Kietzig, Introducing a graphical user interface for dynamic contact angle determination, Phys. Fluids 35 (2023) 072010, https://doi.org/10.1063/5.0154551.
[40] M.B. Asadi, D.G.K. Aboud, M.J. Wood, G. Zeppetelli, A.M. Kietzig, A new insight into dynamic contact angle measurements: implementation of smooth splines method, Colloids Surf. A: Physicochem. Eng. Asp. 655 (2022) 130234, https://doi.org/10.1016/j.colsurfa.2022.130234.
[41] N.K. Andersen, R. Taboryski, Drop shape analysis for determination of dynamic contact angles by double sided elliptical fitting method, Meas. Sci. Technol. 28 (2017) 047003, https://doi.org/10.1088/1361-6501/aa5dcf.
[42] F. Heib, M. Schmitt, Statistical contact angle analyses with the high-precision drop shape analysis (HPDSA) approach: basic principles and applications, Coatings 6 (2016) 57, https://doi.org/10.3390/coatings6040057.
[43] I. Tagliaro, M. Mariani, R. Akbari, M. Contardi, M. Summa, F. Saliu, R. Nisticò, C. Antonini, PFAS-free superhydrophobic chitosan coating for fabrics, Carbohydr. Polym. 333 (2024) 121981, https://doi.org/10.1016/j.carbpol.2024.121981.
[44] S. Brandon, A. Marmur, Simulation of contact angle hysteresis on chemically heterogeneous surfaces, J. Colloid Interface Sci. 183 (1996) 351–355, https://doi.org/10.1006/jcis.1996.0556.
[45] A. Giacomello, L. Schimmele, S. Dietrich, Wetting hysteresis induced by nanodefects, PNAS 113 (2015) E262–E271, https://doi.org/10.1073/pnas.1513942113.
[46] M.A. Sarshar, W. Xu, C.-H. Choi, Correlation between contact line pinning and contact angle hysteresis on heterogeneous surfaces: a review and discussion, in: Adv. Contact Angle, Wettability Adhes., 2013: pp. 1–18, doi: 10.1002/9781118795620.ch1.
[47] K. Grundke, K. Pöschel, A. Synytska, R. Frenzel, A. Drechsler, M. Nitschke, A. L. Cordeiro, P. Uhlmann, P.B. Welzel, Experimental studies of contact angle hysteresis phenomena on polymer surfaces - toward the understanding and control of wettability for different applications, Adv. Colloid Interface Sci. 222 (2015) 350–376, https://doi.org/10.1016/j.cis.2014.10.012.
[48] Y. Jiang, W. Xu, M.A. Sarshar, C.H. Choi, Generalized models for advancing and receding contact angles of fakir droplets on pillared and pored surfaces, J. Colloid Interface Sci. 552 (2019) 359–371, https://doi.org/10.1016/j.jcis.2019.05.053.
[49] X. Zhang, Y. Qin, Contact angle hysteresis of a water droplet on a hydrophobic fuel cell surface, J. Colloid Interface Sci. 545 (2019) 231–241, https://doi.org/10.1016/j.jcis.2019.03.026.
[50] C.W. Extrand, Y. Kumagai, Contact angles and hysteresis on soft surfaces, J. Colloid Interface Sci. 184 (1996) 191–200, https://doi.org/10.1006/jcis.1996.0611.
[51] D. Kim, M. Lee, J.H. Kim, J. Lee, Dynamic contact angle measurements on lubricant infused surfaces, J. Colloid Interface Sci. 586 (2021) 647–654, https://doi.org/10.1016/j.jcis.2020.10.134.
[52] K. Liu, M. Vuckovac, M. Latikka, R.H.A. Ras, Tricky contact angle imaging, Science (80-) 363 (2019) 1147–1148, https://doi.org/10.1126/science.aav5388.
[53] I. Tagliaro, V. Radice, R. Nisticò, C. Antonini, Chitosan electrolyte hydrogel with low ice adhesion properties, Colloids Surf. A: Physicochem. Eng. Asp. 700 (2024), https://doi.org/10.1016/j.colsurfa.2024.134695.
[54] R. Akbari, Y. Wei, A. Bagni, R. Ruffo, M.J. Thoraval, L. Chen, C. Antonini, Outcomes from water drop impact on hydrophobic meshes, Phys. Fluids 36 (2024) 027137, https://doi.org/10.1063/5.0189860.